

Hydrogen- and Halogen-Bonded Binary Cocrystals with Ditopic Components: Systematic Structural and Photoreactivity Properties That Provide Access to a Completed Series of Symmetrical Cyclobutanes

Jay Quentin and Leonard R. MacGillivray*



Cite This: *Cryst. Growth Des.* 2020, 20, 7501–7515



Read Online

ACCESS |



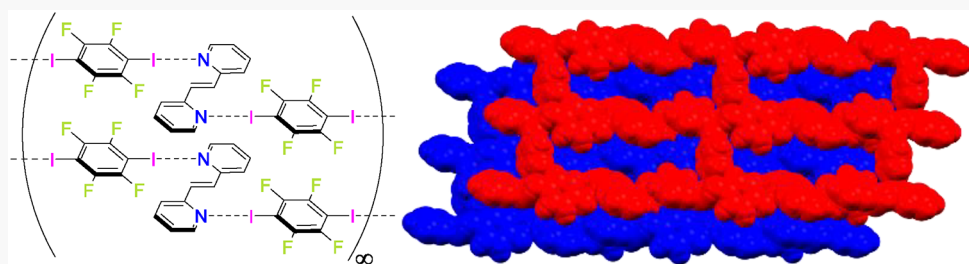
Metrics & More



Article Recommendations



Supporting Information



ABSTRACT: A series of binary cocrystals involving the ditopic hydrogen- and halogen-bond (H- and X-bond, respectively) donors resorcinol (**res**) and hydroquinone (**hq**), and 1,3- and 1,4-diiodotetrafluorobenzene (1,3- and 1,4-**di-I-tFb**), respectively, cocrystallized with one of the three symmetric bipyridines *trans*-1,2-bis(*n*-pyridyl)ethylene (*n,n'*-**bpe**, where $n = n' = 2, 3, 4$) is reported. The structures of the six novel cocrystals, (1,3-**di-I-tFb**)·(3,3'-**bpe**), 4(**res**)·3(3,3'-**bpe**), (1,3-**di-I-tFb**)·(4,4'-**bpe**), 3(**hq**)·2(2,2'-**bpe**), (1,4-**di-I-tFb**)·(3,3'-**bpe**), and (**hq**)·(3,3'-**bpe**), are described. The cocrystals comprise components that assemble by either O–H···N and O–H···O H-bonds (**res** and **hq**) or N···I X-bonds (1,3- and 1,4-**di-I-tFb**). The work completes a series of 18 cocrystals involving either the three dihydroxybenzenes catechol (**cat**), **res**, and **hq** or the three diiodotetrafluorobenzenes (1,2-, 1,3-, and 1,4-**di-I-tFb**) as H- or X-bond donors, respectively, with each of the three structurally isomeric symmetric bipyridines *n,n'*-**bpe**. Our study demonstrates the significant consequences that minimally subtle variations to molecular structure of cofomers can have for stoichiometric formulations, molecular packing, and solid-state photoreactivity. The work also provides access to a completed series of symmetrically substituted *rctt*-tetrakis(*n*-pyridyl)cyclobutanes (where: $n = 2, 3, \text{ or } 4$).

INTRODUCTION

Recent efforts by us have focused on comparisons of hydrogen- (H-) and halogen- (X-) bonding in alkene-containing binary cocrystals.¹ Specifically, our interests are in bifunctional molecules that can serve as building blocks of photoreactive solids. Nature is replete with examples of structural effects of H-bonding that lead to complex form and function. The field of crystal engineering constitutes attempts of chemists to effectively profit from Nature's examples in the designed construction of complex crystalline architectures sustained by relatively weak, noncovalent bonds. While we have many noncovalent bonds at our disposal (e.g., hydrogen-, halogen-, dative-, ionic-, metal-coordination, metallophilic, $\pi\cdots\pi$ stacking), some forces are more developed than others. By far the best understood and likely most frequently employed is the H-bond, with a closely related but yet less studied force being the X-bond.² As for H-bonding, the basis for X-bonding is primarily electrostatic, being an interaction of a Lewis-acid with a Lewis-base. Electrophilic regions of X-bond donors recognize complementary nucleophilic (:Nu) regions (e.g., lone pairs) of

acceptor molecules to form an X-bond ($\delta^+X\cdots Nu^{\delta-}$).^{3,4} X-bonds are comparable to H-bonds in both strength⁵ and role in directing self-assembly of individual molecules into supramolecular structures.⁶ Our group has invoked H-bond^{1,7–10} and X-bond^{11–13} donor molecules (e.g., templates) that support the preorganization of alkene-containing acceptor cofomers into the geometry of Schmidt¹⁴ to undergo solid-state [2 + 2] photocycloadditions that furnish symmetrical 1,2,3,4-tetrasubstituted cyclobutanes. Our successes have led us to examine the topologies of various photoreactive H- and X-bonded cocrystals we have synthesized and motivated our attempts to generate additional photoactive topologies in cocrystals that involve other alkenes as substrates. Success in these endeavors would

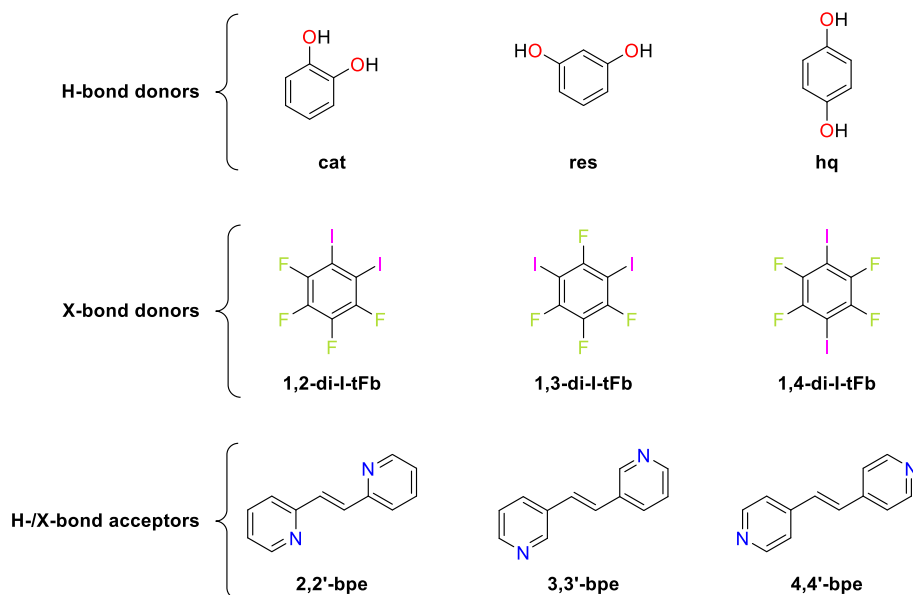
Received: August 21, 2020

Revised: October 4, 2020

Published: October 16, 2020



Scheme 1. Ditopic Components for Cocrystals



constitute an important development in the context of crystal engineering, as H- and X-bonding forces could then be exploited as supramolecular synthons that enable designed topological photodimerizations to furnish targeted cyclobutanes.

The precedent set by H-bonds - and an underlying, comparable capacity of X-bonds - to direct self-assembly of multicomponent systems leads chemists to inquire how topologically similar molecules with H- and X-bonding capabilities can influence self-assembly processes in solids. A proverbial holy grail for crystal engineers is the ability to reliably exploit noncovalent interactions to achieve a functional degree of predictability in the fabrication of solids with desired properties. In this context, the highly directional nature of X-bonds as compared to other noncovalent forces makes them promising candidates for such geometry-based fabrication by design of solids with desired topologies, and—by extension—topology-based properties (e.g., conductivity, reactivity). Despite fundamental geometrical and electronic similarities between H- and X-bonding, relatively few studies exist that directly compare structural effects of the forces on molecular packing.

Experimental,^{15–26} as well theoretical,^{26,27} studies exist with goals to compare influences of H- and X-bonding on self-assembly. The studies can be distilled into three classes: 1) systematic comparisons between H- and X-bonding; 2) competition between H- and X-bonding; and 3) synergistic cooperation of H- and X-bonding. The first class draws comparisons of topologically similar molecules with H- and X-bonding groups that exhibit closely related spatial arrangements. An example is our report¹ comprising a comparison between H- and X-bonding to direct the assembly of cocrystals consisting of structurally analogous H- and X-bond donors. The work was inspired by reports of Metrangolo and Resnati²⁴ involving constitutional isomers of dibromotetrafluorobenzene with a bifunctional alkene. The second class includes a report of Aakeröy that describes organic cocrystals wherein the X-bond donor was varied.¹⁹ The same investigators later described¹⁶ cocrystals that demonstrated consequences of binding-site location on an overall balance between H- and X-bonding.¹⁷ Bosch also described competition between the two interactions

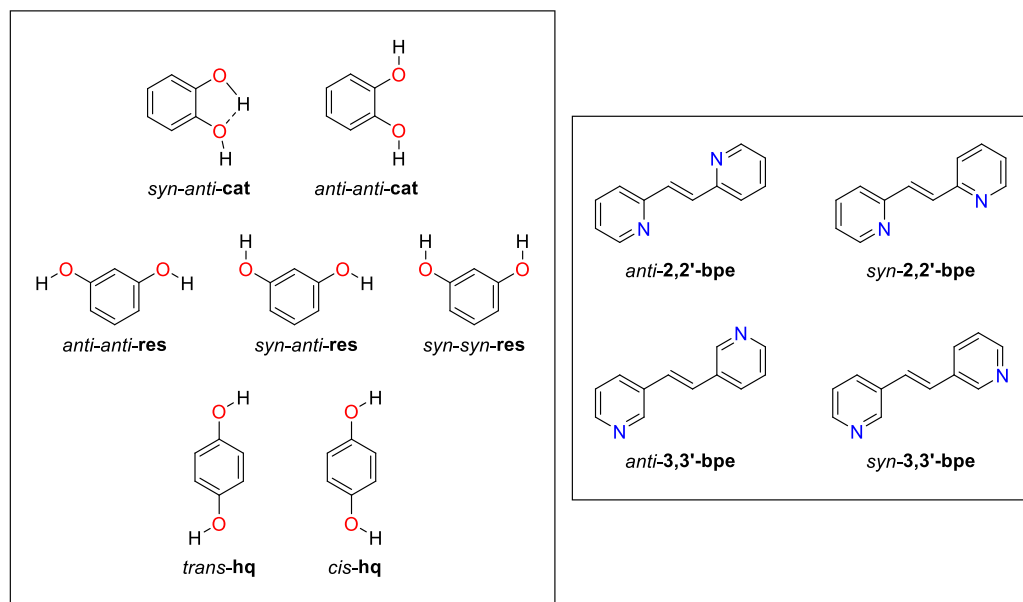
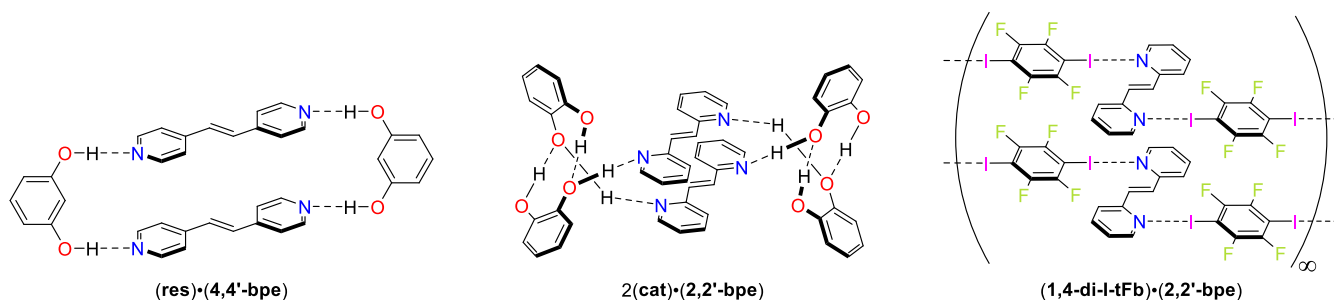
in directing the self-assembly of homodimeric crystals of perfluoroiodo- and perfluorobromophenylethynylpyridines.²⁰ Studies in the third class described cooperativity of H- and X-bond groups. Arman et al. have, thus, reported a cocrystal comprised of a thioamide with **1,2-di-I-tFb** involving both N–H...S H-bonds and Type II²⁸ S...I X-bonds.²¹ Similarly, Uriel demonstrated²³ complementary H- and X-bonding forces in cocrystals of *para*- and *meta*-bis(iodoethynyl)benzene with **4,4'-bpe**.

Here, we report a series of binary cocrystals involving ditopic alkenes and structurally analogous ditopic cofomers with complementary H-bonding (dihydroxybenzenes) and X-bonding (diiodotetrafluorobenzenes) capacities. The three symmetrical constitutional isomers of *n,n'*-**bpe** are the bifunctional acceptors. The three symmetrical constitutional isomers of both dihydroxybenzene and diiodotetrafluorobenzene serve as the H- and X-bond donors, respectively (Scheme 1). Being relatively symmetrical, rigid, conjugated, and generally planar, we expected the cocrystal components to minimize those aspects of encoded molecular information that are typically not amenable to allow for predictable elements of control of crystal packing (e.g., isomerizability, tautomerizability, conformational flexibility, and nitrogen lone-pair inversions,²⁹ to name a few). Our selection of diiodotetrafluorobenzenes as the X-bond donors was informed by the well-established enhancement of X-bond donor capability by poly fluorosubstitution of iodobenzenes.³⁰ An additional advantage of our selected cofomers was that all were commercially available with the exception of **3,3'-bpe**, which was synthesized via a Pd-catalyzed cross-coupling reaction.^{1,31,32} Our efforts here enable us to study a series of 18 cocrystals that we show exhibits remarkable structural diversity in terms of self-assembly and provide all members of the symmetrical *rctt*-1,2,3,4-tetrakis(*n*-pyridyl)-cyclobutanes (*n,n'*-**tpcb**, where *n* = *n'* = 2, 3, or 4).

EXPERIMENTAL SECTION

Materials and Methods. All reagents and solvents (synthesis grade) were purchased from commercial sources and used as received unless otherwise stated. The cocrystal formers **res**, **hq**, **1,4-di-I-tFb** and **4,4'-bpe** were purchased from Aldrich[®]; **2,2'-bpe** was purchased from

Scheme 2. (Left) Stable Planar Rotamers for cat, res, and hq and (Right) Planar Conformers for 2,2'- and 3,3'-bpe

Scheme 3. Photoactive Binary Cocrystals (Left to Right): Discrete, Four-Component (res)·(4,4'-bpe), Discrete, Six-Component 2(cat)·(2,2'-bpe), Face to Face, π -Stacked 1D Chains (1,4-di-I-tFb)·(2,2'-bpe)^a

^aAlkene disorder is omitted for clarity.

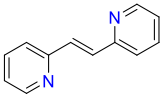
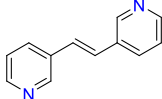
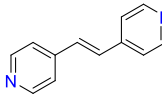
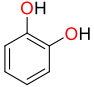
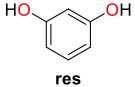
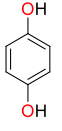
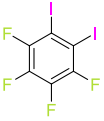
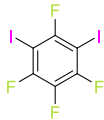
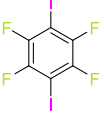
TCI[®]; 1,3-di-I-tFb was purchased from Apollo Scientific[®]. 3,3'-bpe was prepared as described.^{1,31,32} All cocrystal syntheses were conducted in screw-cap glass scintillation vials. The reported cocrystals (res)·(2,2'-bpe),⁷ (res)·(4,4'-bpe),⁷ (hq)·(4,4'-bpe),³³ and (1,4-di-I-tFb)·(4,4'-bpe)³⁰ were prepared as described. We have reported the syntheses of (1,3-di-I-tFb)·(2,2'-bpe) and (1,4-di-I-tFb)·(2,2'-bpe).¹³ The cocrystals (1,3-di-I-tFb)·(3,3'-bpe), 4(res)·3(3,3'-bpe), (1,3-di-I-tFb)·(4,4'-bpe), 3(hq)·2(2,2'-bpe), and (1,4-di-I-tFb)·(3,3'-bpe) were prepared by thermal dissolution of equimolar amounts of the appropriate cofomers. Specifically, both cocrystal components were combined in a vial, solvent was added portion-wise while maintaining a saturated mixture at room temperature, and the vial was tightly capped and heated on a hot-plate until all solids were dissolved so as to afford a homogeneous solution with minimum amount of solvent. The cocrystal (hq)·(3,3'-bpe) was prepared by slow evaporation of a saturated solution of both cocrystal formers in an equimolar ratio at ambient temperature. Photoactivities of the cocrystals were assessed by exposing each solid to UV-radiation in an ACE photocabinet equipped with an ACE quartz, 450 W, broadband, medium pressure, Hg-vapor lamp for a period of 30 h. Compositions of all single crystals were shown to be representative of bulk materials by matching experimental powder X-ray diffraction (pXRD) patterns with those simulated from single-crystal X-ray diffraction (scXRD) data. Cocrystal stoichiometries were determined using scXRD and ¹H NMR spectroscopy where appropriate. pXRD data were collected at room temperature on a Bruker D8 Advance X-ray diffractometer on samples mounted on glass slides. Each sample was finely ground using an agate

mortar-and-pestle prior to mounting. scXRD data were collected on either a Bruker Nonius-Kappa[®] APEX II CCD or a Bruker Nonius-Kappa[®] CCD diffractometer, each equipped with an Oxford Cryosystems 700 series cold N₂ gas stream cooling system. Data were collected at either room temperature (296.15 K) or low temperature (150.15 K) using graphite-monochromated MoK α radiation ($\lambda = 0.71073$ Å). Crystals were mounted in Paratone oil on a MiTeGen[®] magnetic mount. Data collection strategies for ensuring maximum data redundancy and completeness were calculated using the Bruker Apex II software suite. Data collection, initial indexing, frame integration, Lorentz-polarization corrections and final cell parameter calculations were likewise accomplished using the Apex II software suite. Multiscan absorption corrections were performed using SADABS.³⁴ Structure solution and refinement were accomplished using SHELXT³⁵ and SHELXL,³⁶ respectively, within the Olex2³⁷ graphical user interface. Space groups were unambiguously verified using the PLATON³⁸ executable. All non-hydrogen atoms were refined anisotropically. All hydrogen atoms were attached via a riding model at calculated positions using HFIX commands. The occupancies of major and minor positions for disordered C=C bonds for (1,3-di-I-tFb)·(4,4'-bpe) and 3(hq)·2(2,2'-bpe) converged to respective ratios after each was identified in the difference map and freely refined. Figures of all structures were rendered using the CCDC Mercury³⁹ software suite.

RESULTS AND DISCUSSION

Considerations for Self-Assembly. The process of self-assembly relies on geometric parameters encoded at the

Table 1. Binary Cocrystals: Donor:Acceptor Stoichiometry, Primary Assembly Description, Photoactivity, and References

		H-/X-bond acceptor		
		 2,2'-bpe	 3,3'-bpe	 4,4'-bpe
H-/X-bond donor	 cat	2:1; discrete, six-component macrocycle; photoactive ; [10]	1:1; linear chains; photoactive ; [1]	1:1; polar, undulating chains; photostable; [41]
	 res	1:1; discrete, four-component macrocycle; photoactive ; [7]	4:3; 2D rhomboidal grid; photostable; this work	1:1; discrete, four-component macrocycle; photoactive ; [7]
	 hq	3:2; 2D rhomboidal grid; photostable; this work	1:1; linear chains; photostable; this work	1:1; linear chains; photostable; [33]
	 1,2-di-I-tFb	2:1; discrete, three-component assembly; photostable; [1]	2:1; discrete, three-component assembly; photostable; [1]	1:1; zig-zag chains; photostable; [1]
	 1,3-di-I-tFb	1:1; linear chains; photoactive ; [13]	1:1; zig-zag chains; photostable; this work	1:1; wave-like chains; photostable; this work
	 1,4-di-I-tFb	1:1; linear chains; photoactive ; [13]	1:1; wave-like chains; photostable; this work	1:1; linear chains; photostable; [30]

molecular level. In this context, the *meta*- and *para*-disubstitution patterns of a benzene ring provide approximate 120° and 180° angles, respectively, to direct the assembly process (Scheme 2). In contrast to the rigid I-atoms of the X-bond donors 1,*n*-di-I-tFb, the hydroxyl H-atoms of the H-bond

donors cat, res and hq are flexible. Certain rotations of the H-atoms give rise to rotamers for the three dihydroxybenzenes. Rotational barriers to interconversion between rotamers are quite small (<5 kcal·mol⁻¹).⁴⁰ We also note two planar conformational isomers (conformers) each for both 2,2'- and

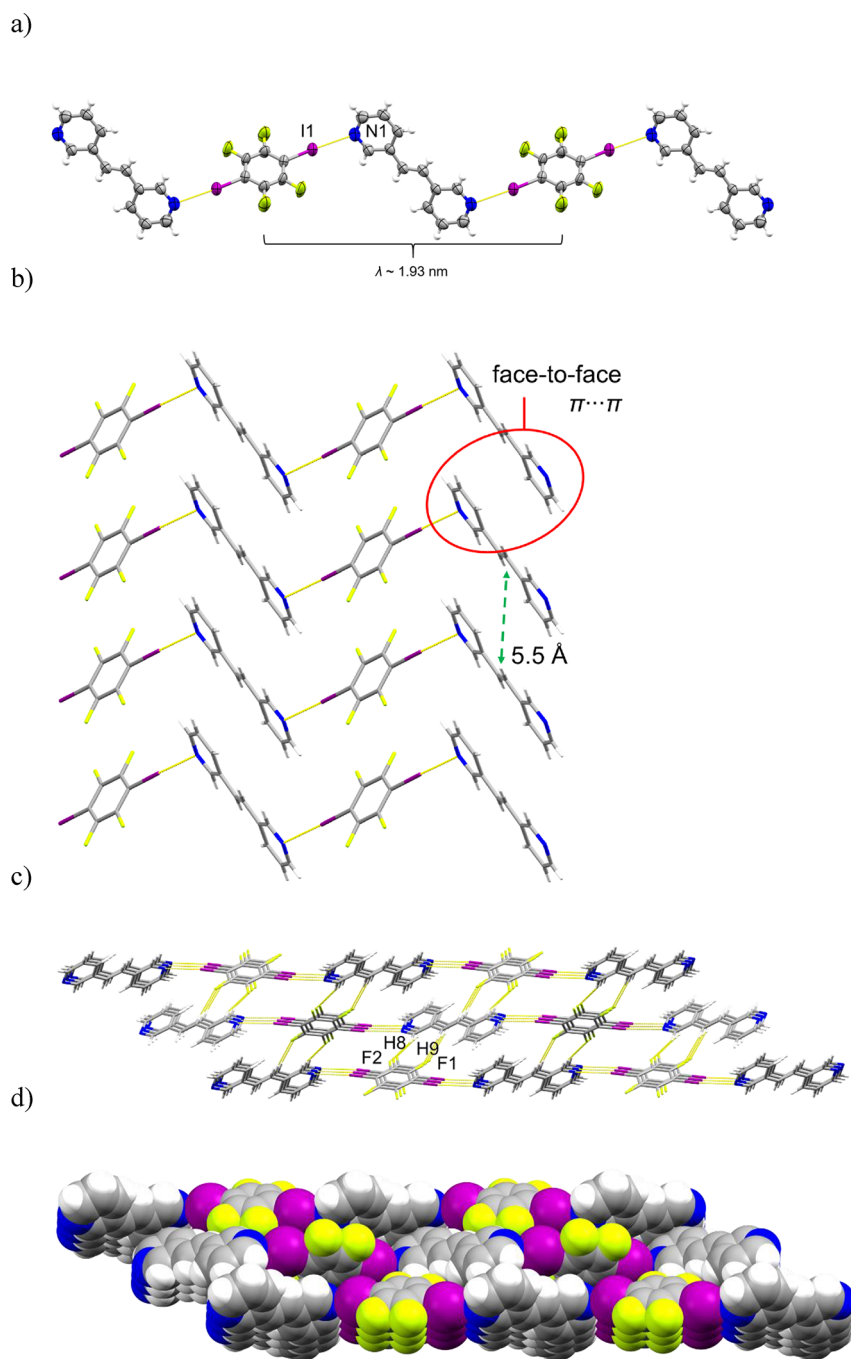


Figure 1. Perspectives of (1,4-di-I-tFb)·(3,3'-bpe): a) wave-like chains; b) herringbone packing of adjacent chains highlighting nearest-neighbor alkene separation (green dashed arrow) and face-to-face $\pi \cdots \pi$ forces (red oval); c) C–H···F interactions between adjacent herringbone assemblies; d) adjacent herringbone assemblies (space-filling).

3,3'-bpe, distinguished by the relative orientations of the N-atoms.

The substitution patterns of the three dihydroxybenzenes and **1,*n*-di-I-tFb** ($n = 2, 3$, or 4) support X- and H-bonded cocrystals involving n,n' -bpe to form either zero- (0D) or one-dimensional (1D) frameworks (Scheme 3). The 0D H-bonded frameworks constitute supramolecular macrocycles with alkene C=C bonds that conform to the criteria of Schmidt¹⁴ to undergo topochemical photodimerization in the solid state. The photoactive 0D frameworks have been achieved in the form of four-component macrocycles involving **res**, an organic template⁷ as the H-bond donor, with either **2,2'-bpe** or **4,4'-bpe** as

the H-bond acceptor alkene. We have also reported photoactive binary cocrystals of both **2,2'-bpe**¹⁰ and **3,3'-bpe**¹ with **cat** as the H-bond donor. The cocrystal involving **2,2'-bpe** involved a six-component, 0D supramolecular macrocycle whereas the solid involving **3,3'-bpe** involved a 1D linear framework. The components formed face-to-face π -stacked columns with nearest-neighbor alkenes within columns preorganized to undergo photodimerization. We have also reported photoactive binary cocrystals of **2,2'-bpe** using **1,3-** and **1,4-di-I-tFb** as X-bond donor cofomers.¹³ When cocrystallized with **2,2'-bpe**, the components formed chains with nearest-neighbor alkenes preorganized in a geometry conducive to photodimerization.

Table 2. Crystallographic Data for (1,4-di-I-tFb)·(3,3'-bpe), (1,3-di-I-tFb)·(4,4'-bpe), and (1,3-di-I-tFb)·(3,3'-bpe)^a

compound	(1,4-di-I-tFb)·(3,3'-bpe)	(1,3-di-I-tFb)·(4,4'-bpe)	(1,3-di-I-tFb)·(3,3'-bpe)
CCDC deposition number	1985188	1985182	1985176
empirical formula	C ₁₈ H ₁₀ F ₄ I ₂ N ₂	C ₁₈ H ₁₀ F ₄ I ₂ N ₂	C ₁₈ H ₁₀ F ₄ I ₂ N ₂
formula weight/g·mol ⁻¹	584.08	584.08	584.08
temperature/K	296.15	296.15	296.15
crystal system	monoclinic	monoclinic	triclinic
space group	<i>P</i> ₂ ₁ / <i>c</i>	<i>P</i> ₂ ₁ / <i>n</i>	<i>P</i> -1
<i>a</i> /Å	11.1810(11)	14.9362(15)	7.9685(8)
<i>b</i> /Å	6.2446(6)	6.1869(6)	10.4506(10)
<i>c</i> /Å	13.6142(14)	20.619(2)	11.6746(12)
α /°	90	90	96.155(5)
β /°	102.044(5)	100.286(5)	97.299(5)
γ /°	90	90	105.554(5)
volume/Å ³	929.63(16)	1874.8(3)	918.80(16)
<i>Z</i>	2	4	2
ρ_{calc} /g·cm ⁻³	2.087	2.069	2.111
μ /mm ⁻¹	3.425	3.396	3.465
<i>F</i> (000)	548	1096	548
crystal size/mm ³	0.26 × 0.18 × 0.1	0.32 × 0.18 × 0.08	0.18 × 0.15 × 0.12
radiation	MoK α (λ = 0.71073)	MoK α (λ = 0.71073)	MoK α (λ = 0.71073)
2 θ range for data collection/°	6.12 to 50	5.544 to 50	5.752 to 50.994
index ranges	-13 ≤ <i>h</i> ≤ 13, -7 ≤ <i>k</i> ≤ 7, -12 ≤ <i>l</i> ≤ 16	-17 ≤ <i>h</i> ≤ 12, -7 ≤ <i>k</i> ≤ 7, -23 ≤ <i>l</i> ≤ 24	-9 ≤ <i>h</i> ≤ 9, -12 ≤ <i>k</i> ≤ 12, -11 ≤ <i>l</i> ≤ 14
reflections collected	4724	9025	5349
independent reflections	1628 [<i>R</i> _{int} = 0.0236, <i>R</i> _{sigma} = 0.0223]	3290 [<i>R</i> _{int} = 0.0274, <i>R</i> _{sigma} = 0.0264]	3407 [<i>R</i> _{int} = 0.0174, <i>R</i> _{sigma} = 0.0322]
data/restraints/parameters	1628/0/118	3290/0/239	3407/0/235
goodness-of-fit on <i>F</i> ²	1.06	1.067	1.054
final <i>R</i> indices [<i>I</i> ≥ 2 σ (<i>I</i>)]	<i>R</i> ₁ = 0.0219 w <i>R</i> ₂ = 0.0532	<i>R</i> ₁ = 0.0254 w <i>R</i> ₂ = 0.0618	<i>R</i> ₁ = 0.0283 w <i>R</i> ₂ = 0.0610
<i>R</i> indices (all data)	<i>R</i> ₁ = 0.0268 w <i>R</i> ₂ = 0.0553	<i>R</i> ₁ = 0.0325 w <i>R</i> ₂ = 0.0649	<i>R</i> ₁ = 0.0456 w <i>R</i> ₂ = 0.0658
largest diff. peak/hole/e·Å ⁻³	0.34/-0.52	0.40/-0.75	0.52/-0.81

$$^a R_1 = \frac{\sum ||F_o| - |F_c||}{\sum |F_o|}, wR_2 = \frac{[\sum w(F_o^2 - F_c^2)^2]}{[\sum w(F_o^2)^2]^{1/2}}. \text{ Goodness-of-fit} = \frac{[\sum w(|F_o| - |F_c|)^2]}{(N_{\text{obs}} - N_{\text{parameter}})^{1/2}}.$$

The reacting C=C bonds of both solids were in a criss-crossed orientation. When subjected to UV-irradiation, all solids reacted to generate the corresponding cyclobutane *n,n'*-**tpcb** (*n* = *n'* = 2, 3, or 4) stereospecifically and quantitatively. The successes to generate either H- or X-bonded cocrystals, coupled with the formation of 0D and 1D photoactive frameworks, inspired us to further explore structural and photoactive properties of binary cocrystals based on the series (Table 1). While the novel cocrystals described here were prepared by combining both cofomers in equimolar amounts, two of the cocrystals crystallized in 3:2 and 4:3 stoichiometries.

Halogen-Bonded Cocrystals. The components of (1,4-di-I-tFb)·(3,3'-bpe), (1,3-di-I-tFb)·(4,4'-bpe), and (1,3-di-I-tFb)·(3,3'-bpe) self-assemble via N⋯I X-bonds. The I-donor atoms are rigid, with the spatial arrangements of the I-donor atoms in 1,3- and 1,4-di-I-tFb being sufficiently distant such that steric crowding can be less expected to disrupt the assembly process versus cocrystals involving 1,2-di-I-tFb.⁴²

Crystal Structure of (1,4-di-I-tFb)·(3,3'-bpe). The components of (1,4-di-I-tFb)·(3,3'-bpe) crystallize in the monoclinic space group *P*₂₁/*c* (Figure 1 and Table 2). The asymmetric unit consists of one half-molecule of 1,4-di-I-tFb and one-half molecule of 3,3'-bpe, both of which lie on crystallographic centers of inversion. The pyridyl (pyr) rings of 3,3'-bpe adopt an *anti* conformation (Figure 1a). The alkene atoms of 3,3'-bpe lie approximately coplanar with the pyr rings (twist angle ~6.4°). The components assemble primarily via N⋯I X-bonds (*d*(N1⋯I1) = 2.958(3) Å) to form wave-like chains (λ ~ 1.93

nm) (Figure 1a). Adjacent chains interact via highly offset, face-to-face π ⋯ π forces between nearest-neighbor pyr rings (*d*(pyr⋯pyr) ~ 5.1 Å) such that adjacent chains stack in a herringbone arrangement along the crystallographic *b*-axis. Nearest-neighbor alkenes of 3,3'-bpe lie stacked parallel and offset, and separated on the order of 5.5 Å (Figure 1b). Adjacent herringbone assemblies stack offset and interact via C-H⋯F forces (Figures 1c,d).

Crystal Structure of (1,3-di-I-tFb)·(4,4'-bpe). The components of (1,3-di-I-tFb)·(4,4'-bpe) crystallize in the monoclinic space group *P*₂₁/*n* (Figure 2 and Table 2). The asymmetric unit consists of one full molecule of 1,3-di-I-tFb and two one-half-molecules of 4,4'-bpe, with the C=C bonds of both alkenes sitting on crystallographic centers of inversion. The alkene atoms of each 4,4'-bpe lie almost perfectly coplanar with the pyr rings (twist angles: ~ 5.4° [N1], ~ 1.4° [N2]). One of the crystallographically unique alkenes (N2) lies disordered over two sites (occupancies: 72/28). The components of (1,3-di-I-tFb)·(4,4'-bpe) assemble via N⋯I X-bonds (*d*(N1⋯I1) = 2.915(3) Å; *d*(N2⋯I2) = 2.879(3) Å) to generate wave-like chains (λ ~ 3.97 nm, Θ ~ 130.7°) (Figure 2a). Within chains, unique molecules of 4,4'-bpe deviate slightly (13.1°) from coplanarity. Adjacent chains run parallel and pack in a herringbone arrangement, interacting via a combination of edge-to-edge C-H⋯F and face-to-face F⋯F forces to form approximately planar sheets (Figure 2b). Nearest-neighbor alkenes for both crystallographically unique molecules of 4,4'-

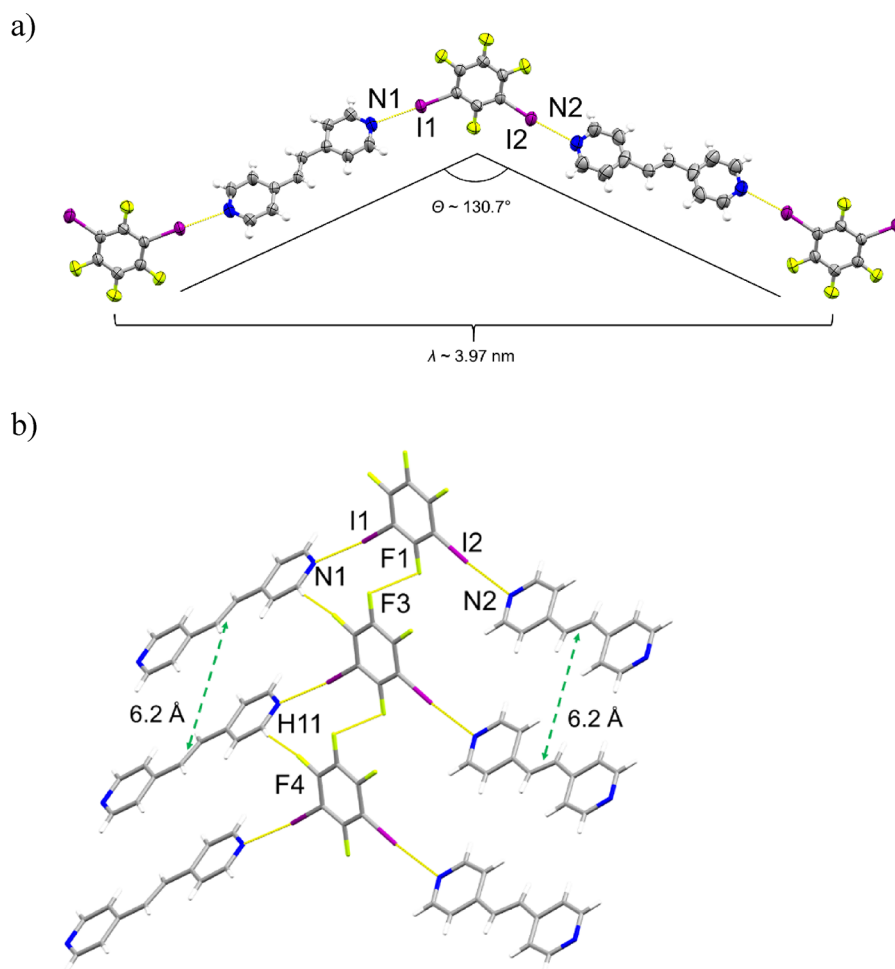


Figure 2. Perspectives of $(1,3\text{-di-I-tFb})\cdot(4,4'\text{-bpe})$ (alkene disorder omitted for clarity): a) wave-like chains; and b) herringbone packing between chains highlighting nearest-neighbor alkene separations (green dashed arrows) (view along c).

bpe (between adjacent chains) lie parallel, highly offset and separated on the order of 6.2 Å (Figure 2b).

Crystal Structure of $(1,3\text{-di-I-tFb})\cdot(3,3'\text{-bpe})$. The components of $(1,3\text{-di-I-tFb})\cdot(3,3'\text{-bpe})$ crystallize in the triclinic space group $P\bar{1}$ (Figure 3 and Table 2). The asymmetric unit consists of one full molecule of **1,3-di-I-tFb** and two half-molecules of **3,3'-bpe**. Both alkene C=C bonds lie on crystallographic centers of inversion. The pyr rings of both molecules of **3,3'-bpe** adopt an *anti* conformation (Figure 3a). The alkene atoms of one molecule of **3,3'-bpe** (N1) are approximately coplanar with the pyr rings (twist angle $\sim 6.2^\circ$), while the alkene atoms of the other **3,3'-bpe** (N2) are appreciably twisted from the plane of the pyr rings (twist angle $\sim 12.0^\circ$). The components assemble via N \cdots I X-bonds ($d(\text{N1}\cdots\text{I1}) = 2.942(4)$ Å; $d(\text{N2}\cdots\text{I2}) = 3.009(3)$ Å) to generate zigzag chains ($\lambda \approx 3.28$ nm, $\Theta \approx 123.4^\circ$) (Figure 3a). Adjacent chains interact via a combination of C–H \cdots F forces and face-to-face π -stacks involving the pyr and alkene carbon atoms of the crystallographically unique, nearest-neighbor **3,3'-bpe** (Figures 3b,c). Alkenes of nearest-neighbor molecules of **3,3'-bpe** (between adjacent chains) are stacked yet highly staggered and separated on the order of 4.0 Å (Figure 3b).

Hydrogen-Bonded Cocrystals. The components of $(\text{hq})\cdot(3,3'\text{-bpe})$, $3(\text{hq})\cdot 2(2,2'\text{-bpe})$, and $4(\text{res})\cdot 3(3,3'\text{-bpe})$ self-assemble, similar to the X-bonded cocrystals, to form extended networks sustained primarily by O–H \cdots N H-bonds. Intermolecular

O–H \cdots O H-bonds are also present in $3(\text{hq})\cdot 2(2,2'\text{-bpe})$ and $4(\text{res})\cdot 3(3,3'\text{-bpe})$.

Crystal structure of $(\text{hq})\cdot(3,3'\text{-bpe})$. The components of $(\text{hq})\cdot(3,3'\text{-bpe})$ crystallize in the triclinic space group $P\bar{1}$ (Figure 4 and Table 3). The asymmetric unit consists of one half-molecule of **3,3'-bpe** and one half-molecule of **hq**, both of which lie on crystallographic centers of inversion. The pyr rings of **3,3'-bpe** adopt an *anti* conformation (Figure 4a). The hydroxyl groups of **hq** adopt a *trans* conformation (Figure 4a). The alkene atoms of **3,3'-bpe** are almost perfectly coplanar with the pyr rings (twist angle $\sim 5.3^\circ$). The components assemble primarily via O–H \cdots N ($d(\text{O1-H1}\cdots\text{N1}) = 2.744(2)$ Å) H-bonds to generate linear chains ($\lambda \approx 1.77$ nm) (Figure 4a). Adjacent chains run parallel and interact via offset, face-to-face $\pi\cdots\pi$ stacking between pyr rings of **3,3'-bpe** ($d(\text{pyr}\cdots\text{pyr}) \approx 4.61$ Å) to generate planar sheets (Figures 4b,c). Nearest-neighbor alkenes of **3,3'-bpe** (between adjacent chains) are parallel but nearly coplanar, are highly offset, and are separated on the order of 9.6 Å (Figure 4b).

Crystal structure of $3(\text{hq})\cdot 2(2,2'\text{-bpe})$. The components of $3(\text{hq})\cdot 2(2,2'\text{-bpe})$ crystallize in the triclinic space group $P\bar{1}$ (Figure 5 and Table 3). The asymmetric unit consists of one full molecule and one half-molecule of **hq** and two half-molecules of **2,2'-bpe** (Figure 5a). The one half-molecule of **hq** and the alkene C=C bonds of both molecules of **2,2'-bpe** lie on crystallographic centers of inversion. The pyr rings of both

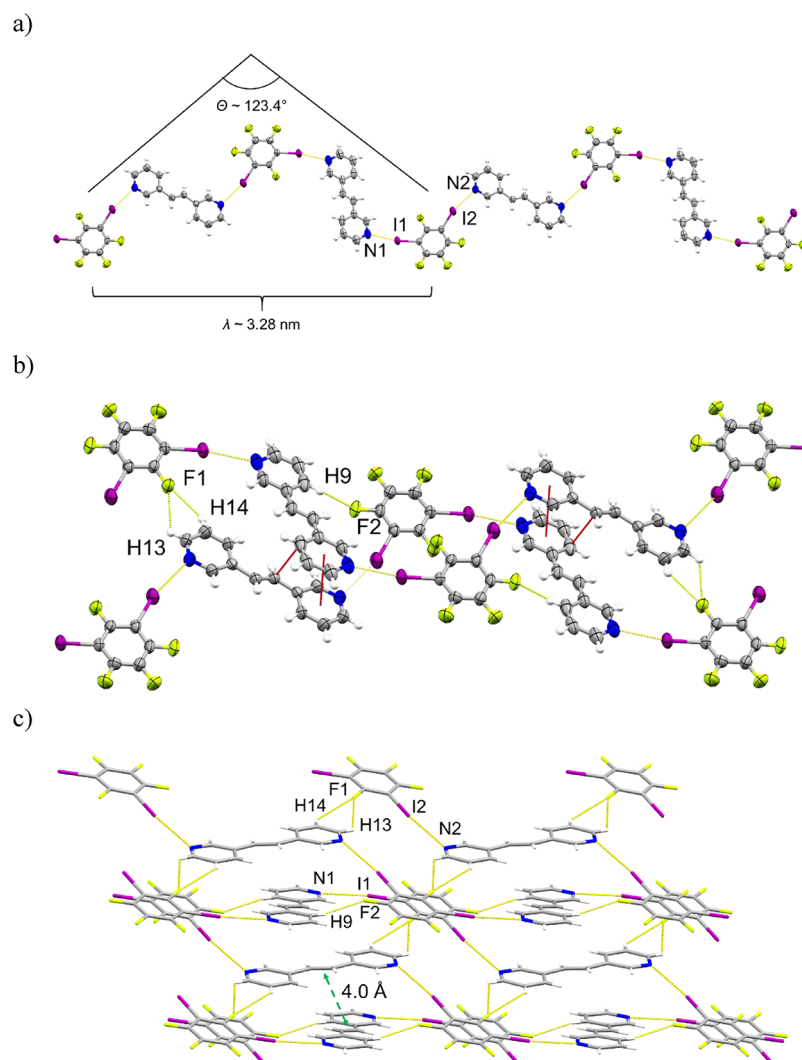


Figure 3. Perspectives of $(1,3\text{-di-I-tFb})\cdot(3,3'\text{-bpe})$: (a) zigzag chains; (b) face-to-face $\pi\cdots\pi$ stacks between chains (red dashed lines); (c) interactions between chains illustrating $\text{C-H}\cdots\text{F}$ contacts and highlighting nearest-neighbor alkene separation (green dashed arrow).

molecules of $2,2'\text{-bpe}$ adopt an *anti* conformation. The hydroxyl groups of the full **hq** molecule (O2/O3) adopt a *trans* conformation (Figure 5a). The alkene atoms of one $2,2'\text{-bpe}$ (N1) are almost perfectly coplanar (twist angle $\sim 2.3^\circ$), whereas the alkene atoms of the other (N2) are appreciably twisted from the plane of the pyr rings (twist angle $\sim 7.4^\circ$). The alkenes of each molecule of $2,2'\text{-bpe}$ are disordered over two sites (occupancies: 88/12 (N1), 88/12 (N2)).

The components assemble via a combination of $\text{O-H}\cdots\text{N}$ ($d(\text{O1-H1}\cdots\text{N1}) = 2.730(2) \text{ \AA}$; $d(\text{O2-H2A}\cdots\text{N2}) = 2.808(2) \text{ \AA}$) and $\text{O-H}\cdots\text{O}$ ($d(\text{O3-H3A}\cdots\text{O1}) = 2.783(2) \text{ \AA}$) H-bonds (Figure 5b) to generate corrugated ($\lambda \approx 11.6 \text{ \AA}$) (Figure 5c) rhomboidal grids (dimensions $11.6 \text{ \AA} \times 21.3 \text{ \AA}$, $\Theta_1 \approx 82.35^\circ$, $\Theta_2 \approx 97.65^\circ$) (Figure 5d). The rhomboidal topology is defined by the centroids of the alkenes. The lengths of the rhomboidal cavities are defined by a bridging alkene and two terminal **hq** molecules. Each pyr group along a length participates in an $\text{O-H}\cdots\text{N-H}$ bond to an **hq** molecule. The remaining hydroxyl group of the **hq** molecule participates in an $\text{O-H}\cdots\text{O}$ H-bond to the second unique **hq** molecules, which serve as the widths. The hydroxyl groups of the **hq** molecules that comprise the width form $\text{O-H}\cdots\text{N}$ H-bonds to the second unique $2,2'\text{-bpe}$ molecules that serve as vertices. The length edge **hq** molecules

also participate in edge-to-face $\text{C-H}\cdots\pi$ interactions with vertex alkenes. Adjacent grids exhibit a tongue-in-groove fit (Figure 5e), stacking parallel, interacting primarily via two edge-to-face $\text{C-H}\cdots\pi$ forces between unique molecules of **hq** ($d(\text{C2}\cdots\text{hq}_{[\text{O2/O3}]}) \approx 3.81 \text{ \AA}$; $d(\text{C3}\cdots\text{hq}_{[\text{O2/O3}]}) \approx 3.86 \text{ \AA}$).

Crystal Structure of $4(\text{res})\cdot 3(3,3'\text{-bpe})$. The components of $4(\text{res})\cdot 3(3,3'\text{-bpe})$ crystallize in the triclinic space group $P\bar{1}$ (Figure 6 and Table 3). The asymmetric unit consists of two full molecules of **res** and three half-molecules of $3,3'\text{-bpe}$ (Figure 6a). The alkenes of all three molecules of $3,3'\text{-bpe}$ sit on crystallographic centers of inversion (Figure 6a), with the pyr rings of each molecule adopting an *anti* conformation (Figure 6b). The hydroxyl groups of both **res** molecules adopt a *syn-anti* conformation. The alkene atoms of one $3,3'\text{-bpe}$ (N3) lie nearly coplanar with the pyr rings (twist angle $\sim 2.7^\circ$), while the alkene atoms of the other two $3,3'\text{-bpe}$ are appreciably twisted (twist angles: $\sim 8.5^\circ$ (N1), $\sim 19.0^\circ$ (N2)).

The components of $4(\text{res})\cdot 3(3,3'\text{-bpe})$ assemble via $\text{O-H}\cdots\text{N}$ ($d(\text{O1-H1}\cdots\text{N1}) = 2.659(2) \text{ \AA}$; $d(\text{O2-H2}\cdots\text{N2}) = 2.822(2) \text{ \AA}$; $d(\text{O3-H3}\cdots\text{N3}) = 2.737(2) \text{ \AA}$) and $\text{O-H}\cdots\text{O}$ ($d(\text{O4-H4}\cdots\text{O1}) = 2.722(2) \text{ \AA}$) H-bonds, as well as $\text{C-H}\cdots\text{O}$ forces (Figure 6b) to generate, similarly to $3(\text{hq})\cdot 2(2,2'\text{-bpe})$, corrugated ($\lambda \approx 22.2 \text{ \AA}$) (Figure 6c) rhomboidal grids (dimensions $13.2 \text{ \AA} \times 22.2$

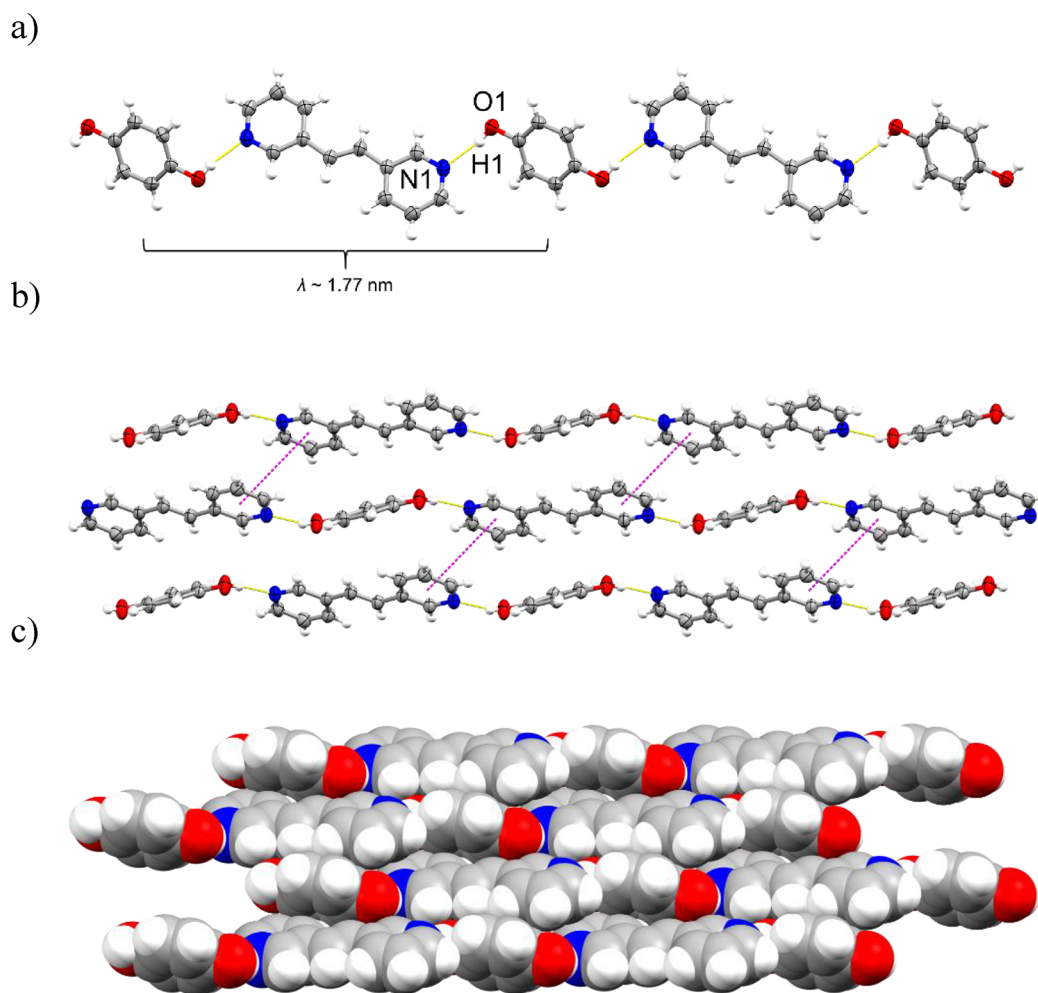


Figure 4. Perspectives of (hq)·(3,3'-bpe): (a) linear chains (view along *b*); (b) planar sheets with offset, face-to-face $\pi \cdots \pi$ stacks highlighted (pink dashed lines); (c) planar sheets (space-filling).

Å, $\Theta_1 \approx 59.34^\circ$, $\Theta_2 \approx 120.66^\circ$) (Figure 6d). The rhomboidal topology can also be defined by the centroids of the alkenes. Thus, a central alkene and two terminal **res** molecules define the widths of cavities and, in contrast to 3(hq)·2(2,2'-bpe), the cavity lengths are defined by bridging alkenes. The vertices are, similarly to 3(hq)·2(2,2'-bpe), defined by an alkene that participates in H-bonds to two **res** molecules (Figure 6d). Adjacent grids exhibit a tongue-in-groove fit (Figure 6e), interacting primarily via C–H···O forces between pyr rings of 3,3'-bpe (N2) and **res** (O3/O4) ($d(\text{C15} \cdots \text{O3}) \sim 3.60$ Å). Nearest-neighbor molecules of 3,3'-bpe (N2, N3) are parallel but severely offset and are separated on the order of 6.6 Å (Figure 6b).

Self-Assembly and Photoreactivity. Our previous work demonstrated that cocrystallizations of **res** with symmetrical n,n' -bpe ($n = n' = 2, 4$) generate discrete, four-component, H-bonded macrocycles with photoactive alkenes.⁷ Cocrystallization of **cat** with symmetrical n,n' -bpe ($n = n' = 2, 3$) was also shown to generate photoactive solids comprising either 0D discrete (2,2'-bpe)⁹ or 1D infinite (3,3'-bpe)¹ assemblies. More recently, we described 1D infinite assemblies in X-bonded cocrystals of 1,*n*-di-I-tFb ($n = 3, 4$) and 2,2'-bpe that are photoactive.¹³

The current work provides an account of all 18 binary cocrystals involving any of the three isomers of the ditopic H- and X-bond donors dihydroxybenzene and diiodotetrafluor-

obenzene, respectively, with the symmetrical and ditopic H- and X-bond acceptors n,n' -bpe ($n = n' = 2, 3, 4$). Extensive work by us has shown the utility of using H-bonded macrocycles to control the [2 + 2] photodimerization using **res** as a template. Given the sensitivity of crystal packing to subtle changes to molecular structure, it is imperative to study the crystal landscape available for structurally analogous components to understand the scope and assess limitations to control organization and reactivity.

The primary interactions that sustain the components in the 18 cocrystals are either O–H···N H-bonds or N···I X-bonds. Intermolecular O–H···O bonds also formed in the H-bonded solids.^{1,7,13} Six of the 18 cocrystals are photoactive, with stacked alkene C=C bonds that generally conform to the principles of Schmidt^{14,43} for solid-state photodimerization. Of the six photoactive cocrystals, half involve infinite and half involve discrete self-assembled structures. The alkene 2,2'-bpe was the most common reactive bipyridine in the series (Table 4 and Figure 7).

Collectively, the ditopic nature of the donor and acceptor molecules tends to support the formation of infinite assemblies, with 13 of the 18 structures being either 1D (11 chains) or 2D (two rhomboidal grids). All cocrystals with the *para*-disubstituted H- and X-bond donors in the form of **hq** and 1,4-di-I-tFb, respectively, formed infinite assemblies. Secondary interactions and steric issues involving the *ortho*- and *meta*-

Table 3. Crystallographic Data for (hq)·(3,3'-bpe), 3(hq)·2(2,2'-bpe), and 4(res)·3(3,3'-bpe)^a

	(hq)·(3,3'-bpe)	3(hq)·2(2,2'-bpe)	4(res)·3(3,3'-bpe)
CCDC deposition no.	1985199	1985203	1985202
empirical formula	C ₁₈ H ₁₆ N ₂ O ₂	C ₂₁ H ₁₉ N ₂ O ₃	C ₃₀ H ₂₇ N ₃ O ₄
formula weight/g mol ⁻¹	292.33	347.38	493.54
temp/K	150.15	296.15	296.15
cryst syst	triclinic	triclinic	triclinic
space group	$P\bar{1}$	$P\bar{1}$	$P\bar{1}$
<i>a</i> /Å	6.1637(6)	9.0992(9)	8.3960(8)
<i>b</i> /Å	7.1041(7)	9.9930(10)	10.9807(11)
<i>c</i> /Å	8.7870(9)	10.8409(11)	15.4072(15)
α /deg	80.619(5)	67.355(5)	109.631(5)
β /deg	77.571(5)	79.380(5)	98.380(5)
γ /deg	86.851(5)	86.527(5)	94.853(5)
volume/Å ³	370.64(6)	894.11(16)	1309.9(2)
Z	1	2	2
$\rho_{\text{calc}}/\text{g cm}^{-3}$	1.31	1.29	1.251
μ/mm^{-1}	0.087	0.087	0.084
<i>F</i> (000)	154	366	520
crystal size/mm ³	0.155 × 0.1 × 0.09	0.3 × 0.21 × 0.2	0.36 × 0.25 × 0.06
radiation	Mo K α (λ = 0.71073)	Mo K α (λ = 0.71073)	Mo K α (λ = 0.71073)
2 θ range for data collection/deg	4.806–55.764	5.592–47.996	3.98–49.998
index ranges	−8 ≤ <i>h</i> ≤ 8, −9 ≤ <i>k</i> ≤ 9, −9 ≤ <i>l</i> ≤ 11	−10 ≤ <i>h</i> ≤ 10, −11 ≤ <i>k</i> ≤ 11, −12 ≤ <i>l</i> ≤ 10	−9 ≤ <i>h</i> ≤ 9, −12 ≤ <i>k</i> ≤ 13, −15 ≤ <i>l</i> ≤ 18
no. of rflns collected	5110	4587	7275
no. of indep rflns	1708 (<i>R</i> _{int} = 0.0226, <i>R</i> _{σ} = 0.0245)	2782 (<i>R</i> _{int} = 0.0210, <i>R</i> _{σ} = 0.0320)	4582 (<i>R</i> _{int} = 0.0205, <i>R</i> _{σ} = 0.0355)
no. of data/restraints/params	1708/0/101	2782/0/245	4582/0/338
goodness of fit on <i>F</i> ²	1.035	1.047	1.059
final <i>R</i> indices (<i>I</i> ≥ 2 σ (<i>I</i>))	<i>R</i> ₁ = 0.0424 <i>wR</i> ₂ = 0.1092	<i>R</i> ₁ = 0.0414 <i>wR</i> ₂ = 0.1086	<i>R</i> ₁ = 0.0436 <i>wR</i> ₂ = 0.1023
<i>R</i> indices (all data)	<i>R</i> ₁ = 0.0490 <i>wR</i> ₂ = 0.1136	<i>R</i> ₁ = 0.0531 <i>wR</i> ₂ = 0.1159	<i>R</i> ₁ = 0.0669 <i>wR</i> ₂ = 0.1113
largest diff peak, hole/e Å ⁻³	0.18, −0.17	0.16, −0.14	0.20, −0.16

^a*R*₁ = $\sum ||F_o| - |F_c|| / \sum |F_o|$. *wR*₂ = $[\sum w(F_o^2 - F_c^2)^2] / [\sum (w(F_o^2)^2)]^{1/2}$. Goodness of fit = $[\sum w(|F_o| - |F_c|)^2] / (N_{\text{obs}} - N_{\text{parameter}})]^{1/2}$.

Table 4. Photoreactive Cocrystals Involving *n,n'*-bpe

H-/X-bond acceptor	no. of photoreactive structures
2,2'-bpe	4
3,3'-bpe	1
4,4'-bpe	1

disubstitution patterns of the ditopic donor molecules supported the formation of finite (i.e., 0D) assemblies. We are unaware of a cocrystal that exhibits a rhomboidal topology, although grid frameworks are known for reticular⁴⁴ structures involving covalent^{45,46} and metal–organic^{47,48} frameworks (COFs and MOFs, respectively). The formation of the grids here involves H-bonded aggregates of molecules that define vertices of the grid structures. That aggregates, as opposed to single molecules, define the vertices attests to the structural versatility of the H-bonded assembly process to support an infinite assembly process. The aggregates correspond to two of the four cocrystals that do not exhibit a 1:1 stoichiometry (Figure 7 and Table 5). A 1:1 stoichiometry was most common among the solids (13 instances, 72%).

From an organic synthesis standpoint, each of the three symmetrical cyclobutane isomers of *n,n'*-tpcb is made available within the series of 18 cocrystals. A combination of *cat* and *res* provide access to each member of the cyclobutane series. X-bonded cocrystals based on 1,*n*-di-*I*-tFb (*n* = 3, 4) generate only 2,2'-tpcb. We also note that each cocrystal-based synthesis provides a highly step economical⁴⁹ (less than or equal to three

steps) and relatively cost economical⁵⁰ access to a cyclobutane photoproduct. With the sole exception of 3,3'-bpe—which is prepared via a one-pot, aqueous Pd-catalyzed Hiyama–Heck cross-coupling^{1,31,32}—all cocrystal components are commercially available. Moreover, each synthesis is perfectly redox economical⁴⁸ and—owing to the ease of separation and recovery of the auxiliary H-/X-bond donors following photodimerization—also perfectly atom economical.⁴⁹ The work is of significant synthetic utility for the reliable and efficient generation of symmetrical *rctt*-1,2,3,4-tetrakis(*n*-pyridyl)-cyclobutanes.

CONCLUSIONS

In this contribution, we have synthesized and structurally characterized six binary cocrystals sustained by either intermolecular H- or X-bonds. Each of the three isomers of the symmetric bipyridine *n,n'*-bpe form cocrystals with each of three isomers of both dihydroxybenzene and diiodotetrafluorobenzene, which function as H- and X-bond donors, respectively. Our work, in combination with previous reports that span the past two decades, provides a series of 18 cocrystals of ditopic H- and X-bonding components. Structural diversity is represented in the series (i.e., 0D, 1D, and 2D assemblies), providing elements of both predictability and discovery in the outcomes of the solid-state assembly processes. An important utility is that the cocrystals provide efficient access to a series of cyclobutane photoproducts. We now aim to utilize the structural and reactivity data to set a path to develop a more

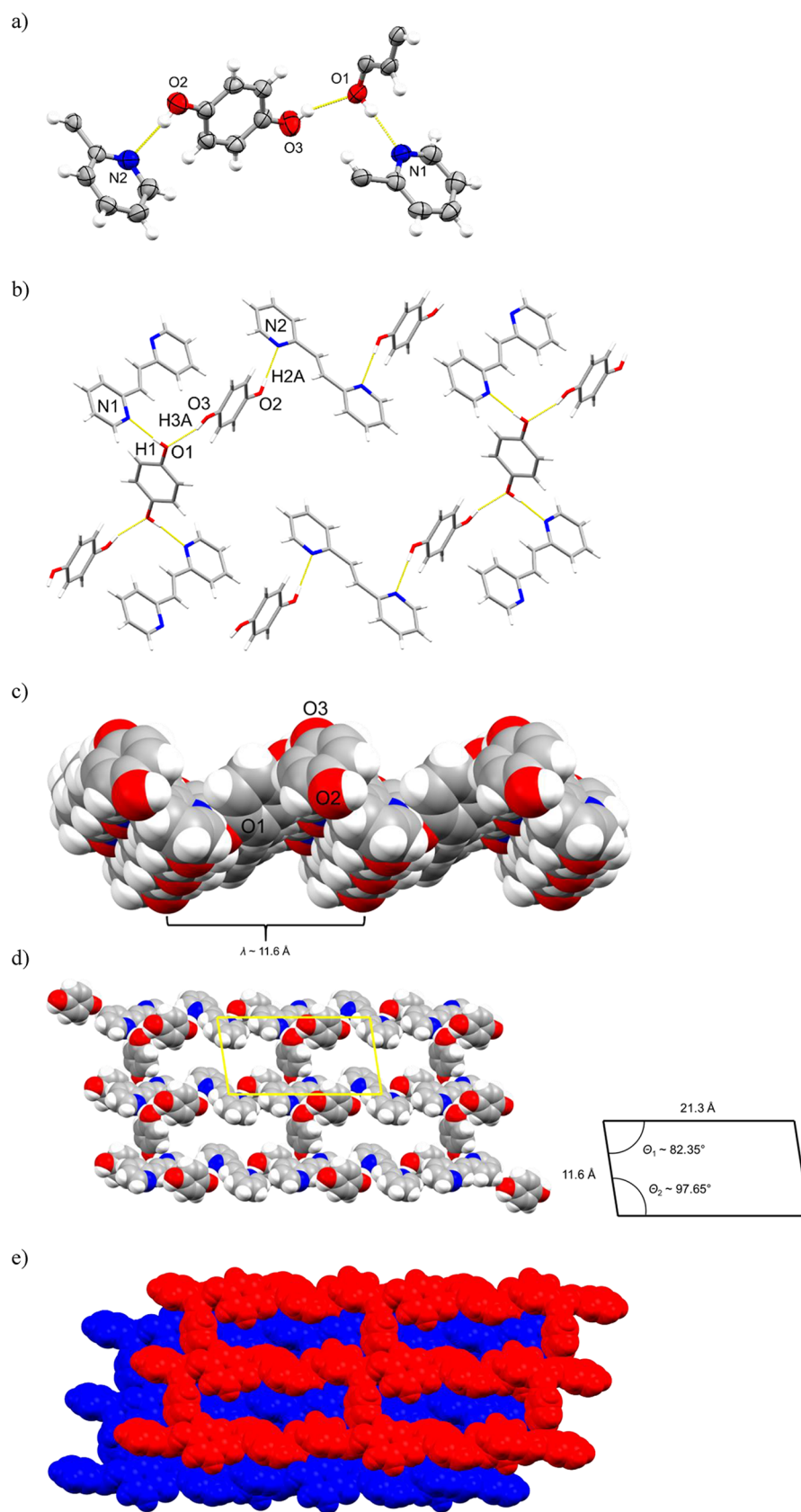


Figure 5. Perspectives of $3(\text{hq}) \cdot 2(2,2'\text{-bpe})$ (alkene disorder omitted for clarity): (a) asymmetric unit; (b) intermolecular forces O–H...N and O–H...O H bonds; (c) edge-on view of corrugated sheets (space-filling); (d) sheets (space filling) consisting of rhomboidal grids (highlighted yellow) with parameters for rhomboidal unit shown at right; (e) tongue-in-groove stacking of grids (space filling).

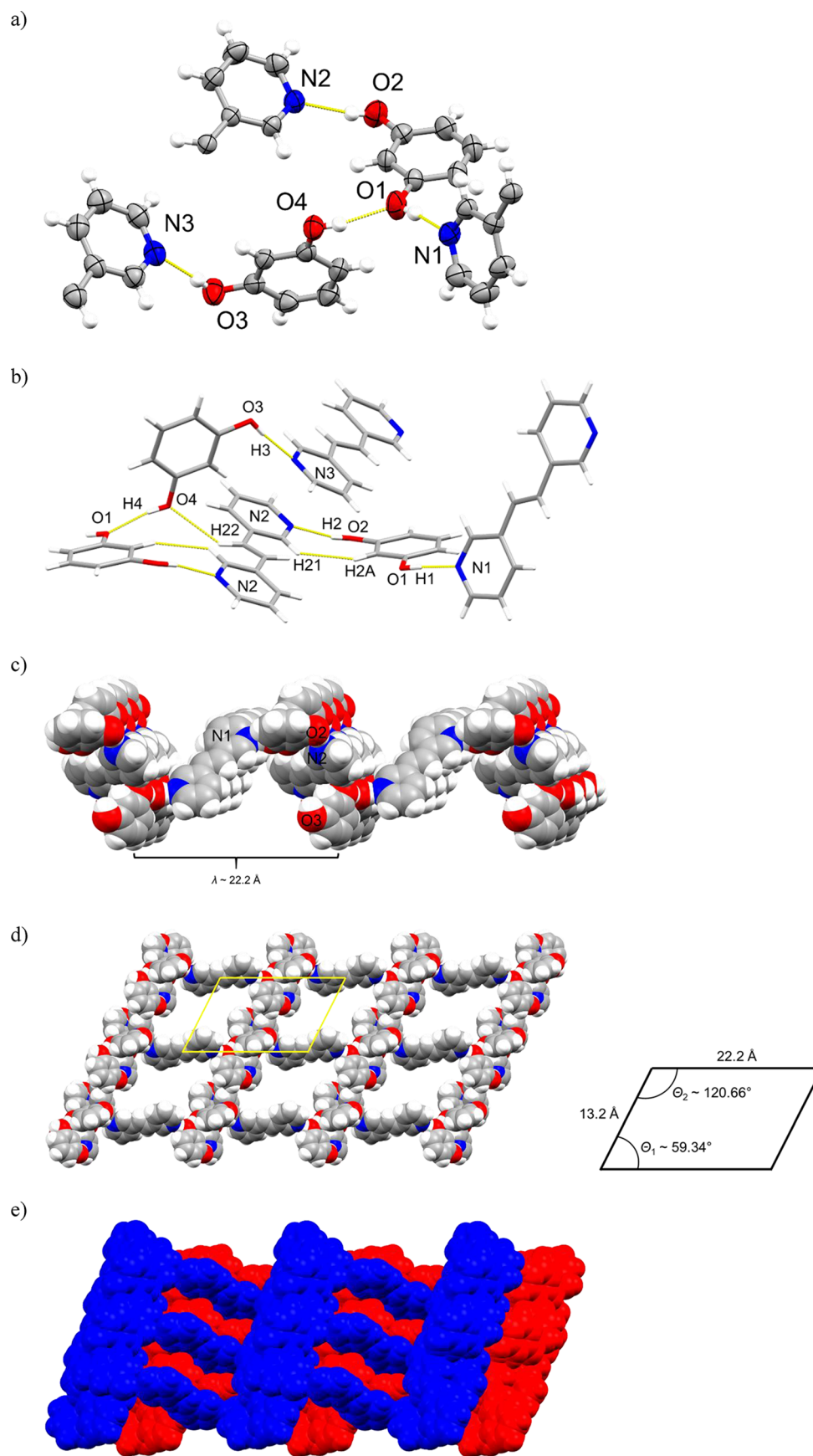


Figure 6. Perspectives of 4(res)·3(3,3'-bpe): (a) asymmetric unit; (b) intermolecular forces O—H...N and O—H...O H bonds and edge-to-edge C—H...H; (c) edge-on view of corrugated sheets (space filling); (d) rhomboidal grid (space filling) with parameters for the rhomboidal unit (highlighted yellow) shown on the right; (e) tongue-in-groove stacking of grids (space filling).

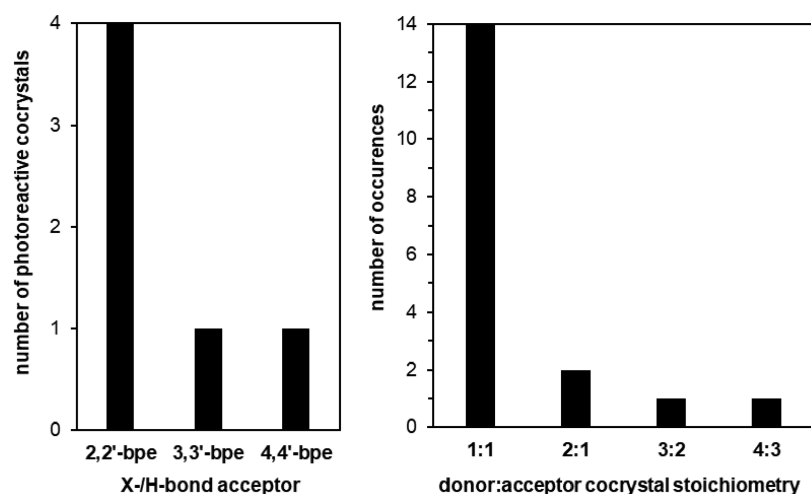


Figure 7. Histograms: (left) photoreactive cocrystals with n,n' -bpe; (right) cocrystal stoichiometries.

Table 5. Donor:Acceptor Cocrystal Stoichiometries for (Left) Ditopic H-/X-Bond Acceptors and (Right) Ditopic H-/X-Bond Donors

H-/X-bond acceptor	donor:acceptor stoichiometric ratio				H-/X-bond donor disubstitution pattern	donor:acceptor stoichiometric ratio			
	1:1	2:1	3:2	4:3		1:1	2:1	3:2	4:3
2,2'-bpe	3	2	1		<i>ortho</i> (cat, 1,2-di-I-tFb)	3	3		
3,3'-bpe	4	1		1	<i>meta</i> (res, 1,3-di-I-tFb)	5			1
4,4'-bpe	6				<i>para</i> (hq, 1,4-di-I-tFb)	5		1	
sum	13	3	1	1	sum	13	3	1	1

comprehensive understanding of X- versus H-bonding forces and the consequences for supramolecular structure, self-assembly, and solid-state reactivity.

■ ASSOCIATED CONTENT

Supporting Information

The Supporting Information is available free of charge at <https://pubs.acs.org/doi/10.1021/acs.cgd.0c01143>.

General experimental details, synthetic procedures for 3,3'-bpe, (res)·(2,2'-bpe), (1,3-di-I-tFb)·(3,3'-bpe), 4(res)·3(3,3'-bpe), (1,3-di-I-tFb)·(4,4'-bpe), (res)·(4,4'-bpe), 3(hq)·2(2,2'-bpe), (1,4-di-I-tFb)·(3,3'-bpe), (hq)·(3,3'-bpe), (1,4-di-I-tFb)·(4,4'-bpe), and (hq)·(4,4'-bpe), ¹H NMR spectra for: 4(res)·(3,3'-bpe), 3(hq)·2(2,2'-bpe), and (hq)·(3,3'-bpe), pXRD patterns for (res)·(2,2'-bpe), (1,3-di-I-tFb)·(3,3'-bpe), 4(res)·3(3,3'-bpe), (1,3-di-I-tFb)·(4,4'-bpe), (res)·(4,4'-bpe), 3(hq)·2(2,2'-bpe), (1,4-di-I-tFb)·(3,3'-bpe), (hq)·(3,3'-bpe), (1,4-di-I-tFb)·(4,4'-bpe), (hq)·(4,4'-bpe), and (1,3-di-I-tFb)·(3,3'-bpe), crystallographic data and structure refinement statistics for 4(res)·3(3,3'-bpe), (1,3-di-I-tFb)·(4,4'-bpe), 3(hq)·2(2,2'-bpe), (1,4-di-I-tFb)·(3,3'-bpe), and (hq)·(3,3'-bpe), hydrogen bond metrics for all nine H-bonded cocrystals, bond metrics for all nine X-bonded cocrystals, melting point data for all nine H-bonded cocrystals and cofomers thereof, and melting point data for all nine X-bonded cocrystals and cofomers thereof (PDF)

Accession Codes

CCDC 1985176, 1985182, 1985188, 1985199, and 1985202–1985203 contain the supplementary crystallographic data for this paper. These data can be obtained free of charge via www.ccdc.cam.ac.uk/data_request/cif, or by emailing data_request@ccdc.cam.ac.uk, or by contacting The Cambridge Crystallographic Data Centre, 12 Union Road, Cambridge CB2 1EZ, UK; fax: +44 1223 336033.

request@ccdc.cam.ac.uk, or by contacting The Cambridge Crystallographic Data Centre, 12 Union Road, Cambridge CB2 1EZ, UK; fax: +44 1223 336033.

■ AUTHOR INFORMATION

Corresponding Author

Leonard R. MacGillivray – Department of Chemistry, University of Iowa, Iowa City, Iowa 52242, United States; orcid.org/0000-0003-0875-677X; Email: len-macgillivray@uiowa.edu

Author

Jay Quentin – Department of Chemistry, University of Iowa, Iowa City, Iowa 52242, United States; orcid.org/0000-0002-1729-7774

Complete contact information is available at: <https://pubs.acs.org/10.1021/acs.cgd.0c01143>

Author Contributions

The manuscript was written through contributions of all authors. All authors have given approval to the final version of the manuscript.

Notes

The authors declare no competing financial interest.

■ ACKNOWLEDGMENTS

We gratefully acknowledge financial support from the National Science Foundation (L.R.M., DMR-1708673).

■ ABBREVIATIONS

H-bond, hydrogen bond; X-bond, halogen bond; cat, catechol; res, resorcinol; hq, hydroquinone; 1,*n*-di-I-tFb, 1,*n*-diiodotetrafluorobenzene; 1,2-di-I-tFb, 1,2-diiodotetrafluorobenzene; 1,3-di-I-tFb, 1,3-diiodotetrafluorobenzene; 1,4-di-I-tFb, 1,4-di-

dotetrafluorobenzene; *n,n'*-bpe, *trans*-1,2-bis(*n*-pyridyl)ethylene; 2,2'-bpe, *trans*-1,2-bis(2-pyridyl)ethylene; 3,3'-bpe, *trans*-1,2-bis(3-pyridyl)ethylene; *n,n'*-tpcb, *rcctt*-1,2,3,4-tetrakis(*n*-pyridyl)cyclobutane; 2,2'-tpcb, *rcctt*-1,2,3,4-tetrakis(2-pyridyl)cyclobutane; 3,3'-tpcb, *rcctt*-1,2,3,4-tetrakis(3-pyridyl)cyclobutane; 4,4'-tpcb, *rcctt*-1,2,3,4-tetrakis(4-pyridyl)cyclobutane; pXRD, powder X-ray diffraction; scXRD, single-crystal X-ray diffraction; ¹H NMR, proton nuclear magnetic resonance; pyr, pyridine or pyridyl

REFERENCES

- (1) Quentin, J.; MacGillivray, L. R. Halogen versus Hydrogen Bonding in Binary Cocrystals: Novel Conformation a Cofomer with [2 + 2] Photoreactivity of Criss-Crossed C=C Bonds. *ChemPhysChem* **2020**, *21*, 154–163.
- (2) Desiraju, G. R.; Ho, P. S.; Kloo, L.; Legon, A. C.; Marquardt, R.; Metrangolo, P.; Politzer, P. A.; Resnati, G.; Rissanen, K. Definition of the Halogen Bond (IUPAC Recommendations 2013). *Pure Appl. Chem.* **2013**, *85*, 1711–1713.
- (3) Murray, J. S.; Riley, K. E.; Politzer, P.; Clark, T. Directional Weak Intermolecular Interactions: σ -Hole Bonding. *Aust. J. Chem.* **2010**, *63*, 1598–1607.
- (4) Clark, T.; Hennemann, M.; Murray, J.; Politzer, P. Halogen Bonding: the σ -Hole. *J. Mol. Model.* **2007**, *13*, 291–296.
- (5) Awwadi, F. F.; Taher, D.; Haddad, S. F.; Turnbull, M. M. Competition between Hydrogen and Halogen Bonding Interactions: Theoretical and Crystallographic Studies. *Cryst. Growth Des.* **2014**, *14*, 1961–197.
- (6) Metrangolo, P.; Resnati, G. Halogen Versus Hydrogen. *Science* **2008**, *321*, 918–919.
- (7) MacGillivray, L. R.; Reid, J. L.; Ripmeester, J. A. Supramolecular Control of Reactivity in the Solid State Using Linear Molecular Templates. *J. Am. Chem. Soc.* **2000**, *122*, 7817–7818.
- (8) Oburn, S. M.; Quentin, J.; MacGillivray, L. R. A Divergent Alkyne Diol Directs [2 + 2] Photoreactivity in the Solid State: Cocrystal, Supramolecular Catalysis, and Sublimation Effects. *Molecules* **2019**, *24*, 3059.
- (9) Campillo-Alvarado, G.; Brannan, A. D.; Swenson, D. C.; MacGillivray, L. R. Exploiting the Hydrogen-Bonding Capacity of Organoboronic Acids to Direct Covalent Bond Formation in the Solid State: Templatation and Catalysis of the [2 + 2] Photodimerization. *Org. Lett.* **2018**, *20*, 5490–5492.
- (10) Papaefstathiou, G. S.; Duncan, A. J. E.; MacGillivray, L. R. Two Act as One: Unexpected Dimers of Catechol Direct a Solid-State [2 + 2] Photodimerization in a Six-Component Hydrogen-Bonded Assembly. *Chem. Commun.* **2014**, *50*, 15960–15962.
- (11) Sinnwell, M. A.; MacGillivray, L. R. Halogen-Bond-Templated [2 + 2] Photodimerization in the Solid State: Directed Synthesis and Rare Self-Inclusion of a Halogenated Product. *Angew. Chem., Int. Ed.* **2016**, *55*, 3477–3480.
- (12) Sinnwell, M. A.; Blad, J. N.; Thomas, L. R.; MacGillivray, L. R. Structural Flexibility of Halogen Bonds Showed in a Single-Crystal-to-Single-Crystal [2 + 2] Photodimerization. *IUCrJ* **2018**, *5*, 491–496.
- (13) Quentin, J.; Swenson, D. C.; MacGillivray, L. R. Supramolecular Sandwiches: Halogen-Bonded Cofomers Direct [2 + 2] Photoreactivity in Two-Component Cocrystals. *Molecules* **2020**, *25*, 907.
- (14) Schmidt, G. M. J. Photodimerization in the Solid State. *Pure Appl. Chem.* **1971**, *27*, 647–678.
- (15) Awwadi, F. F.; Haddad, S. F.; Willett, R. D.; Twamley, B. The Analogy of C–Br···Br–C, C–Br···Br–Fe, and Fe–Br···Br–Fe Contacts: Crystal Structures of (26DAPH)FeBr₄ and (26DA35DBPH)₂FeBr₄·Br. *Cryst. Growth Des.* **2010**, *10*, 158–164.
- (16) Aakeröy, C. B.; Panikkattu, S.; Chopade, P. D.; Desper, J. Competing Hydrogen-Bond and Halogen-Bond Donors in Crystal Engineering. *CrystEngComm* **2013**, *15*, 3125–3136.
- (17) Voth, A. R.; Hays, A. F.; Ho, P. S. Directing Macromolecular Conformation Through Halogen Bonds. *Proc. Natl. Acad. Sci. U. S. A.* **2007**, *104*, 6188–6193.
- (18) Zordan, F.; Brammer, L.; Sherwood, P. Supramolecular Chemistry of Halogens: Complementary Features of Inorganic (M–X) and Organic (C–X') Halogens Applied to M–X···X'–C Halogen Bond Formation. *J. Am. Chem. Soc.* **2005**, *127*, 5979–5989.
- (19) Aakeröy, C. B.; Fasulo, M.; Schultheiss, N.; Desper, J.; Moore, C. Structural Competition between Hydrogen Bonds and Halogen Bonds. *J. Am. Chem. Soc.* **2007**, *129*, 13772–13773.
- (20) Oburn, S. M.; Bowling, N. P.; Bosch, E. Formation of Self-Complementary Halogen-Bonded Dimers. *Cryst. Growth Des.* **2015**, *15*, 1112–1118.
- (21) Arman, H. D.; Gieseking, R. L.; Hanks, T. W.; Pennington, W. T. Complementary Halogen and Hydrogen Bonding: Sulfur···Iodine Interactions and Thioamide Ribbons. *Chem. Commun.* **2010**, *46*, 1854–1856.
- (22) Aakeröy, C. B.; Chopade, P. D.; Ganser, C.; Desper, J. Facile Synthesis and Supramolecular Chemistry of Hydrogen Bond/Halogen Bond-Driven Multi-Tasking Tectons. *Chem. Commun.* **2011**, *47*, 4688–4690.
- (23) Gonzalez, L.; Tejedor, R. M.; Royo, E.; Gaspar, B.; Munarriz, J.; Chanthapally, A.; Serrano, J. L.; Vittal, J. J.; Uriel, S. Two-Dimensional Arrangements of Bis(haloethynyl)benzenes Combining Halogen and Hydrogen Interactions. *Cryst. Growth Des.* **2017**, *17*, 6212–6223.
- (24) De Santis, A.; Forni, A.; Liantonio, R.; Metrangolo, P.; Pilati, T.; Resnati, G. N···Br Halogen Bonding: One-Dimensional Infinite Chains through the Self-Assembly of Dibromotetrafluorobenzenes with Dipyridyl Derivatives. *Chem. - Eur. J.* **2003**, *9*, 3974–3983.
- (25) Legon, A. C. The Interaction of Dihalogens and Hydrogen Halides with Lewis Bases in the Gas Phase: An Experimental Comparison of the Halogen Bond and the Hydrogen Bond. In *Halogen Bonding. Structure and Bonding*; Metrangolo, P., Resnati, G., Eds.; Springer: Berlin, 2007; Vol. 126.
- (26) Geboes, Y.; De Proft, F.; Herrebout, W. A. Towards a Better Understanding of the Parameters Determining the Competition Between Bromine Halogen Bonding and Hydrogen Bonding: An FTIR Spectroscopic Study of the Complexes Between Bromodifluoromethane and Trimethylamine. *J. Mol. Struct.* **2018**, *1165*, 349–355.
- (27) Li, Q.; Jing, B.; Li, R.; Liu, Z.; Li, W.; Luan, F.; Cheng, J.; Gong, B.; Sun, J. Some Measures for Making Halogen Bonds Stronger Than Hydrogen Bonds in H₂CS–HOX (X = F, Cl, and Br) Complexes. *Phys. Chem. Chem. Phys.* **2011**, *13*, 2266–2271.
- (28) Sakurai, T.; Sundaralingam, M.; Jeffrey, G. A. A Nuclear Quadrupole Resonance and X-Ray Study of Crystal Structure of 2,5-Dichloroaniline. *Acta Crystallogr.* **1963**, *16*, 354–363.
- (29) Ammer, J.; Baidya, M.; Kobayashi, S.; Mayr, H. Nucleophilic Reactivities of Tertiary Alkylamines. *J. Phys. Org. Chem.* **2010**, *23*, 1029–1035.
- (30) Walsh, R. B.; Padgett, C. W.; Metrangolo, P.; Resnati, G.; Hanks, T. W.; Pennington, W. T. Crystal Engineering through Halogen Bonding: Complexes of Nitrogen Heterocycles with Organic Iodides. *Cryst. Growth Des.* **2001**, *1*, 165–175.
- (31) Gordillo, A.; Ortuño, M. A.; Lopez-Mardomingo, C.; Lledos, A.; Ujaque, G.; de Jesus, E. Mechanistic Studies on the Pd-Catalyzed Vinylation of Aryl Halides with Vinylalkoxysilanes in Water: The Effect of the Solvent and NaOH Promoter. *J. Am. Chem. Soc.* **2013**, *135*, 13749–13763.
- (32) Gordillo, A.; de Jesús, E.; López-Mardomingo, C. Consecutive Palladium-Catalyzed Hiyama-Heck Reactions in Aqueous Media Under Ligand-Free Conditions. *Chem. Commun.* **2007**, 4056–4058.
- (33) Weyna, D. R.; Shattock, T.; Vishweshwar, P.; Zaworotko, M. J. Synthesis and Structural Characterization of Cocrystals and Pharmaceutical Cocrystals: Mechanochemistry vs Slow Evaporation from Solution. *Cryst. Growth Des.* **2009**, *9*, 1106–1123.
- (34) Otwinowski, Z.; Minor, W. Processing of X-Ray Diffraction Data Collected in Oscillation Mode. *Methods Enzymol.* **1997**, *276*, 307–326.

- (35) Sheldrick, G. M. SHELXT - Integrated Space-Group and Crystal-Structure Determination. *Acta Crystallogr., Sect. A: Found. Adv.* **2015**, *A71*, 3–8.
- (36) Sheldrick, G. M. Crystal Structure Refinement with SHELXL. *Acta Crystallogr., Sect. C: Struct. Chem.* **2015**, *C71*, 3–8.
- (37) Dolomanov, O. V.; Bourhis, L. J.; Gildea, R. J.; Howard, J. A. K.; Puschmann, H. OLEX2: A Complete Structure Solution, Refinement and Analysis Program. *J. Appl. Crystallogr.* **2009**, *42*, 339–341.
- (38) Spek, A. L. Structure Validation in Chemical Crystallography. *Acta Crystallogr., Sect. D: Biol. Crystallogr.* **2009**, *D65*, 148–155.
- (39) Macrae, C. F.; Bruno, I. J.; Chisholm, J. A.; Edgington, P. R.; McCabe, P.; Pidcock, E.; Rodriguez-Monge, L.; Taylor, R.; van de Streek, J.; Wood, P. A. Mercury CSD 2.0 - New Features for the Visualization and Investigation of Crystal Structures. *J. Appl. Crystallogr.* **2008**, *41*, 466–470.
- (40) Puebla, C.; Ha, T.-K. A Theoretical Study of Conformations and Rotational Barriers in Dihydroxybenzenes. *J. Mol. Struct.: THEOCHEM* **1990**, *204*, 337–351.
- (41) Papaefstathiou, G.; Friščić, T.; MacGillivray, L. R. An Infinite Hydrogen-Bonded Molecular Assembly Based on Catechol and a Bifunctional Olefin. *ACA Trans.* **2004**, *39*, 110–113.
- (42) Bedeković, N.; Stilinović, V.; Friščić, T.; Cinčić, D. Comparison of Isomeric *meta*- and *para*-Diiodotetrafluorobenzene as Halogen Bond Donors in Crystal Engineering. *New J. Chem.* **2018**, *42*, 10584–10591.
- (43) Ramamurthy, V.; Sivaguru, J. Supramolecular Photochemistry as a Potential Synthetic Tool: Photocycloaddition. *Chem. Rev.* **2016**, *116*, 9914–9993.
- (44) Yaghi, O. M. Reticular Chemistry—Construction, Properties, and Precision Reactions of Frameworks. *J. Am. Chem. Soc.* **2016**, *138*, 15507–15509.
- (45) Nguyen, H. L.; Hanikel, N.; Lyle, S. J.; Zhu, C.; Proserpio, D. M.; Yaghi, O. M. A Porous Covalent Organic Framework with Voided Square Grid Topology for Atmospheric Water Harvesting. *J. Am. Chem. Soc.* **2020**, *142*, 2218–2221.
- (46) Colson, J. W.; Woll, A. R.; Mukherjee, A.; Levendorf, M. P.; Spitler, E. L.; Shields, V. B.; Spencer, M. G.; Park, J.; Dichtel, W. R. Oriented 2D Covalent Organic Framework Thin Films on Single-Layer Graphene. *Science* **2011**, *332*, 228–231.
- (47) Liu, G.-I.; Song, J.-B.; Qiu, Q.-m.; Li, H. Syntheses, Structures, and Magnetic Properties of Three Supramolecular Isomeric Cu(II) Square Grid Networks: Solvents Effect on the Ligand Linkages. *CrystEngComm* **2020**, *22*, 1321–1329.
- (48) Hudson, T. A.; Sutton, A. L.; Abrahams, B. F.; D'Alessandro, D. M.; Davies, C. G.; Goerigk, L.; Jameson, G. N. L.; Moubaraki, B.; Murray, K. S.; Robson, R.; Usov, P. M.; Yang, G. A Semiconducting Cationic Square-Grid Network with Fe^{III} Centers Displaying Unusual Dynamic Behavior. *Eur. J. Inorg. Chem.* **2020**, *2020*, 1255–1259.
- (49) Newhouse, T.; Baran, P. S.; Hoffmann, R. W. The Economies of Synthesis. *Chem. Soc. Rev.* **2009**, *38*, 3010–3021.
- (50) Berger, O.; Winters, K. R.; Sabourin, A.; Dzyuba, S. V.; Montchamp, J.-L. On the Cost of Academic Methodologies. *Org. Chem. Front.* **2019**, *6*, 2095–2108.